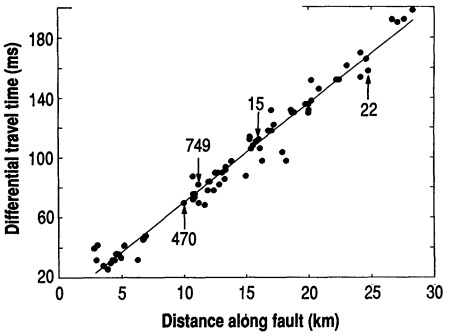

Fig. 6. Time difference between direct and head wave arrivals at MM during the 75 microearthquakes of Fig. 3 plotted against the distance the waves travel along the fault. The events of Figs. 4 and 5 are indicated by arrows. The line shows a least-squares fit of Eq. 2 through the data, indicating a roughly 4% average material contrast across the San Andreas fault at Parkfield.

head wave interpretation. At station GP an up step of a secondary head wave follows the down motion of the direct arrival.

The time difference between fault zone head waves and direct arrivals is approximately

$$\Delta t \sim r[(1/\alpha_2) - (1/\alpha_1)] \sim r(\Delta\alpha/\alpha^2) \quad (2)$$

so that the time separation between the head waves and direct arrivals scales with the distance traveled along the fault. If the arrivals can be correctly identified and timed, the slope $[\Delta t(r_2) - \Delta t(r_1)]/(r_2 - r_1)$ of their time difference versus distance can be used to estimate the average velocity contrast across the fault.

Figure 5 illustrates the data used to examine the time-distance scaling of fault zone head waves and direct arrivals. In the top trace ($r \sim 10$ km) the head wave is a short emergent pulse, truncated by the closely following sharper direct P wave with initial motion of opposite polarity. As the distance from the source increases, the head wave broadens considerably, whereas the direct wave continues to be a relatively sharp, opposite-polarity arrival. The time difference against distance for such first arriving head waves and secondary direct waves for our data (Fig. 6) has a slope

$$s \sim \Delta\alpha/\alpha^2 \sim 0.007 \text{ s/km} \quad (3)$$

For $\alpha = 5.5$ km/s in Eq. 3, the velocity contrast, $\Delta\alpha/\alpha$, across the San Andreas fault near Parkfield is approximately 4%. This value is similar to the contrast used to calculate the expected critical distances of Table 1. We thus propose that, on the basis of travel times, waveforms, and signal polarities, the emergent first arrivals seen at Parkfield are best explained in terms of fault zone head waves. If so, then other types of refracted head waves are also likely to occur. Examples are shear-mode head waves and mode-converted P to S and S to P refractions.

The fault zone head waves are confined to small regions in the vicinity of material interfaces such as the San Andreas fault and are therefore seemingly of local interest only. However, it is precisely the data from these regions that contain the details of earthquake processes and fault zone structure. Fault zone head waves can be mistakenly attributed to various source and medium effects. For example, a head wave propagating along the material interface with P wave velocity and then continuing into the faster medium as an S wave can have a short lag time after the initial P arrival, resulting in a complicated initial waveform. Such waveforms may lead to an assumption of a complex source behavior (for instance, a multiple-slip event). The complexity of the initial P waveforms in the earthquakes we examined increases from the northern station ST to the southern station FR (see, for example, Fig. 4). This increase in complexity may result in part from converted head waves separating in time from the direct P arrival as the source-receiver distance increases. As another example, a head wave that started as a P wave, converted to an S wave, and then continued to an observation point might have a predominantly SV motion, whereas the direct S wave may be characterized (for a strike-slip event) by a predominantly SH motion. The different travel times and motion polarities may be taken as evidence for shear wave splitting arising from anisotropy.

Our study indicates that fault zone head waves are common in the Parkfield seismograms recorded on the slower side of the fault. Fault zone head waves may have both negative and positive effects. On the negative side, misidentification of these phases as direct arrivals introduces errors in event location, earthquake mechanism, and other rupture process and medium property studies. On the positive side, proper analysis of fault zone head waves can be used to study material contrast across important structures such as the San Andreas fault. Careful monitoring of these phases may provide information on variation of fault zone material properties in time and space.

REFERENCES AND NOTES

1. Y. Ben-Zion, *Geophys. J. Int.* **98**, 213 (1989).
2. ———, *ibid.* **101**, 507 (1990).
3. ———, thesis, University of Southern California, Los Angeles (1990).
4. P. E. Malin, S. N. Blakeslee, M. G. Alvarez, A. J. Martin, *Science* **244**, 557 (1989).
5. R. S. Carmichael, Ed., *Handbook of Physical Properties of Rocks* (CRC Press, Boca Raton, FL, 1982), vol. 2.
6. A. W. Walter and W. D. Mooney, *Bull. Seismol. Soc. Am.* **72**, 1567 (1982).
7. J. H. Lees and P. E. Malin, *J. Geophys. Res.* **95**, 21793 (1990).

8. This work was funded by National Science Foundation grant EAR-8904259 (Y.B.-Z.) and U.S. Geological Survey grant 14-08-0001-G1793 (P.M.).

7 November 1990; accepted 24 January 1991

Microtektites, Microkrystites, and Spinels from a Late Pliocene Asteroid Impact in the Southern Ocean

STANLEY V. MARGOLIS,* PHILIPPE CLAEYS, FRANK T. KYTE

The properties of glassy spherules found in sedimentary deposits of a late Pliocene asteroid impact into the southeast Pacific are similar to those of both microtektites and microkrystites. These spherules probably formed from molten silicate droplets that condensed from an impact-generated vapor cloud. The spherules contain inclusions of magnesioferrite spinels similar to those in spherules found at the Cretaceous-Tertiary boundary, indicating that both sets of spherules are impact debris formed under similar physical and chemical conditions.

STUDIES OF LATE PLIOCENE DEEP-SEA sediments (*1–3*) have shown that ~2.3 million years ago an asteroid ~0.5 km in diameter impacted the subantarctic South Pacific Ocean in the region ~1400 km due west of Cape Horn. Sediment deposits recording this impact are enriched in Ir and Au and contain relatively coarse-grained (1 to 5 mm) impact debris. Most of this debris is a vesicular impact melt, composed of asteroidal material and traces of seawater salt from the oceanic impact. A small amount of the debris is unmelted fragments of the impacting mesosiderite asteroid. These fragments have been named the Eltanin meteorite. The deposits indicate that the impact was into the ocean basin, without significant excavation of sea-floor materials or incorporation of marine sediments or oceanic basement into the impact melt (*2*). We describe

S. V. Margolis and P. Claeys, Department of Geology, University of California, Davis, CA 95616.
F. T. Kyte, Institute of Geophysics and Planetary Physics, University of California, Los Angeles, CA 90024.

*To whom correspondence should be addressed.

in this report a new type of impact-produced object associated with this event: glassy spherules, which have properties analogous to those of other impact-derived spherules in the sedimentary record. Examination of material such as this is critical to an understanding of processes that affect the mineralogical and chemical composition of silicate impact debris.

Glassy spherules were recovered from sediments in piston cores E13-3 and E13-4 in the southeastern subantarctic sector of the Pacific Ocean. In E13-3, spherules were recovered at sediment depths of 782 to 793 cm, coincident with previously reported high concentrations of vesicular impact melt (*2*). In E13-4, spherules were most concentrated in samples from depths of 1288 to 1294.6 cm. This is slightly higher in the core than the depth of the peak concentration of coarse (>1 mm) vesicular debris, which was sampled between 1296 and 1298.6 cm depth, immediately above a disconformity (*3*). This separation of the two components of fallout debris in E13-4 may reflect different settling times after the impact (*3*). Most recovered spherules range from ~50 to 200 μm, although one was as large as 350 μm. The spherules are a minor component of the impact debris, constituting <1% of the total fallout material. To date, we have recovered ~200 spherules from these sediment cores for analysis (*4*).

The spherules are shiny submetallic gray to dark black or reddish-brown. Their shapes range from nearly perfect spheres to teardrops, dumbbells, compound spherules, and unusual morphologies, such as glassy stringers (Fig. 1). Compound spherules, consisting of two or more spheres fused together, are abundant, and nearly all of the spherules observed exhibited at least one small attached droplet.

The surface of spherules observed in the scanning electron microscope were found to exhibit different degrees of seawater dissolution of the original features. Some spherules probably retain most of their original surface features: smooth glassy surfaces with only fine-scale etching and preservation of small (~5 μm) attached glass droplets (Fig. 1, D and E). The surfaces of other surfaces appear moderately to severely etched. Some are almost entirely coated with micrometer-sized spinel crystals, presumably exposed by differential dissolution of glass. Others have rough surfaces with pits, perhaps suggesting dissolution of precursors minerals (for example, olivine) near the surface (Fig. 1F). In

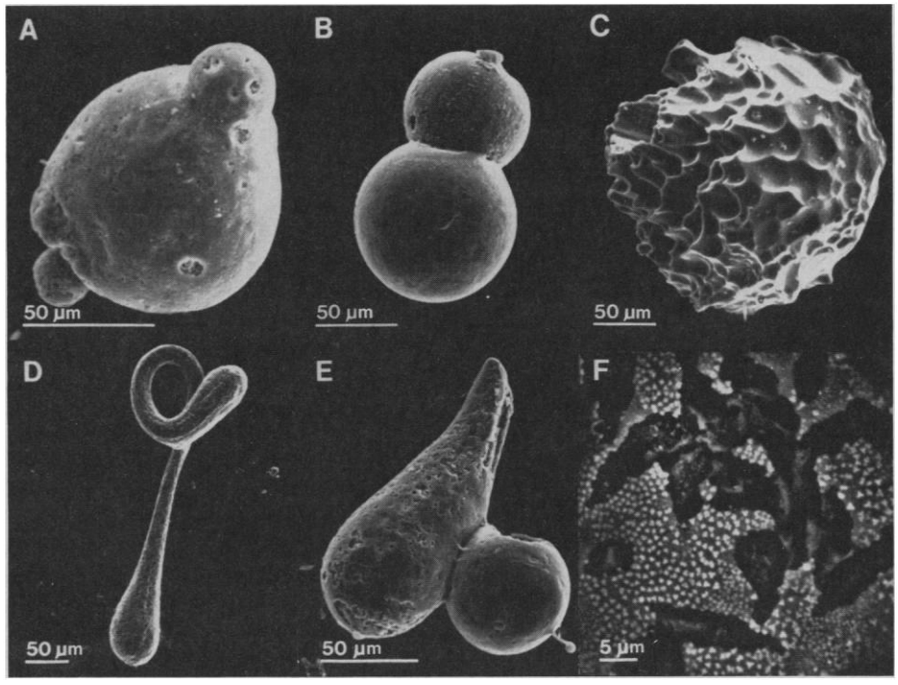

Fig. 1. Scanning electron micrographs of surfaces of glassy, impact-generated spherules from deep-sea sediment cores E13-3 and E13-4. (**A**) Pitted sphere with two attached smaller spherules. (**B**) Compound glassy spherules with fine etched spinel and pits on the surface; note melt welding at the junction. (**C**) Microtektite-like glassy object with etch-sculpted surface, due to seawater solution. (**D**) Elongated stringer-shaped glass particle. (**E**) Compound teardrop-shaped object with an attachment sphere that has a small delicate melted glass projection on the lower right. (**F**) Spherule with spinel crystals on the surface and deeply etched pits.

Table 1. Microprobe analyses of late Pliocene spherules, vesicular melt, and K-T boundary spherules (*6*). The number of analyses is given in parentheses. Fe_2O_3 calculations are based on spinel stochiometry. Data set 1, composition of magnesioferrite spinel from late Pliocene spherules. Data set 2, analyses of chromite spinel in late Pliocene vesicular debris. Also present, but present, but much less abundant and not reported here, are low-Mg magnetite and Ti-rich chromite. Data set 3, composition of spinels contained in K-T boundary spherules from Furlo, Italy (*9*). Data set 4, late Pliocene spherule glass compositions. Data set 5, late Pliocene vesicular impact melt bulk composition (*2*). ND, not determined.

Components	Data set 1		Data set 2		Data set 3		Date set 4		Data set 5, average (%) (7)
	Average (%) (12)	Range (%)	Average (%) (9)	Range (%)	Average (%) (127)	Range (%)	Average (%) (144)	Range (%)	
Na_2O	ND		ND		ND		5.00	1.11–9.10	2.20
MgO	16.19	15.28–18.85	1.89	1.55–2.07	9.86	0.01–17.92	15.26	9.86–18.55	13.80
Al_2O_3	4.94	4.34–5.94	8.05	8.00–8.10	3.38	0.43–10.21	10.48	7.60–17.61	7.80
SiO_2	1.07	0.38–1.55	0.16	0.03–0.4	0.02	0.00–0.06	45.00	41.11–49.88	45.30
K_2O	ND		ND		ND		0.06	0.01–0.11	0.15
CaO	0.36	0.24–0.55	0.15	0.12–0.18	0.39	0.05–1.14	9.65	7.62–15.20	5.70
TiO_2	0.29	0.19–0.54	3.96	3.85–4.10	0.51	0.18–3.56	0.42	0.30–0.61	0.38
Cr_2O_3	3.45	0.46–6.32	50.49	49.32–51.37	0.66	0.07–12.52	ND		ND
MnO	0.67	0.50–0.82	0.74	0.66–0.82	1.15	0.24–2.41	0.39	0.24–0.53	0.47
FeO	1.5	0.00–2.87	29.41	28.98–29.44	9.9	2.05–31.98	14.12	9.84–18.03	23.40
Fe_2O_3	66.21	63.94–69.43	5.41	4.60–5.94	68.44	58.72–72.10	All Fe as FeO		All Fe as FeO
NiO	4.55	2.67–5.75	0.12	0.00–0.36	5.48	0.82–10.17	ND		ND
Total	99.22		100.38		99.79		100.38		100.99

extreme cases, spherule surfaces are sculpted (Fig. 1C) in a manner similar to microtektites (*5*).

In polished section (Fig. 2), spherules were found to be composed primarily of a basaltic glass, commonly with minor spinel crystallites. Microprobe analyses of the glass indicate that the bulk composition is similar to that reported for the vesicular impact melt (Table 1). Neutron activation analysis (NAA) of spherules (*4*) also indicates that the trace elemental compositions of the spherules are similar to those reported for vesicular impact melt except for one notable difference: Ir concentrations in the spherules are 1/30 of those in the vesicular debris (Table 2). Relatively low Ti and high Cr and Mn contents of the glass are characteristic of the impact debris and distinctive from what is observed in terrestrial basalts (*2*).

Typical glass contents of the spherules range from 80 to 100%, although in a few spherules glass contents were as low as ~40 to 50%. Most crystallites of spinel occur near the rims of spherules (Fig. 2, C and D), although some are in the interior. Moreover, the presence of etched pits near spherule rims are suggestive of a precursor dendritic- or spinifex-textured olivine (Fig. 2, B and D). Olivine is an abundant phase in the associated vesicular debris (*2*) and in many cases appears to be preferentially etched out of the altered portions of this material. Some spherules are entirely glass, and these invariably have the heavily sculpted surface features typical of microtektites (Figs. 1C and 2A).

Spinel crystallites occur in a variety of dendritic, equant, and skeletal textures (Fig. 2, C, D, and E) and range in size from <1 to ~4 μm in diameter; a few are as much as 10 μm wide (Fig. 2, C and E). The spinel compositions (*6*) are unlike those for oxides in terrestrial basalts (*7*) in that they have concentrations of Mg, Ni, and Cr and relatively low concentrations of Ti (Table 1); they are Ni- and Cr-rich magnesioferrites. These spinels contrast with spinels in the vesicular debris, which are Fe-rich chromites (Table 1). Interestingly, the spherule spinels are similar in composition and morphology to spinels found in Cretaceous-Tertiary (K-T) boundary spherules, particularly those from European localities [(*8–11*); Fig. 2F and Table 1]. Although the composition of K-T boundary spinels varies regionally (*9*), they are invariably magnesioferrites with low Ti concentrations and significant amounts of Ni. Also, the high Fe_2O_3/FeO ratios of both spinel occurrences are suggestive of relatively high O fugacities during formation (*9, 12*).

The spherule textures observed in this study grade from pure glasses with sculpted surfaces similar to those of typical microtektites (*5*) to crystallite-bearing spherules, which some investigators (*13*) have called microkrystites, although these late Pliocene spherules bear little resemblance to microkrystites of late Eocene age. The latter are highly crystallized with clinopyroxene as the major phase and contain only rare oxides: a chromite spinel (*13*).

We infer that the late Pliocene impact spherules formed in an environment distinctly different from that of the vesicular debris. The absence of vesicles suggests that volatile contents were low during their formation. Different spinel compositions in the two types of debris (spherules and vesicular impact melt; Table 1), in spite of similar bulk chemistry, indicate that environmental conditions during crystallization were most likely more oxidizing for the spherules than for the vesicular debris. The textures of minerals in the two types of debris are also distinct. The vesicular debris is highly crystallized with zoned, equant olivine as the principal phase and common, unmelted meteorite inclusions (*2*). In contrast, the etched crystallites that we presume were olivine in the spherules are a minor component and have dendritic, sometimes spinifex textures. The spherules probably formed from initially hotter, but more rapidly quenched material.

The high abundance of compound spherules indicates that these objects formed in a region with a high density of glassy molten droplets, distinctly different from the region of vesicular impact melt formation. Ablation of asteroid fragments during atmospheric entry is an unlikely source for the spherules, as high Na contents (and detectable Cl) in the glass matrix indicate that they were intimately mixed with salts from the seawater target after impact. A more likely source is molten silicate droplets condensing from the cloud of vaporized projectile and target material. These late Pliocene spherules, associated vesicular impact melt, and unmelted meteorite fragments thus represent products of vapor-, liquid-, and solid-phase ejecta from an asteroid impact into the ocean.

The close similarity of spinel compositions for both the late Pliocene and K-T

Table 2. Comparison of the trace element composition of impact spherules measured by NAA to that of vesicular melt (average of five particles) (*2*).

Element	Vesicular melt	Glassy spherules
Sc (μg/g)	19	19
Cr (mg/g)	5.3	2.2
Fe (mg/g)	139	163
Co (μg/g)	113	131
Ni (μg/g)	1.9	2.4
La (μg/g)	2.1	1.7
Ir (ng/g)	173	5

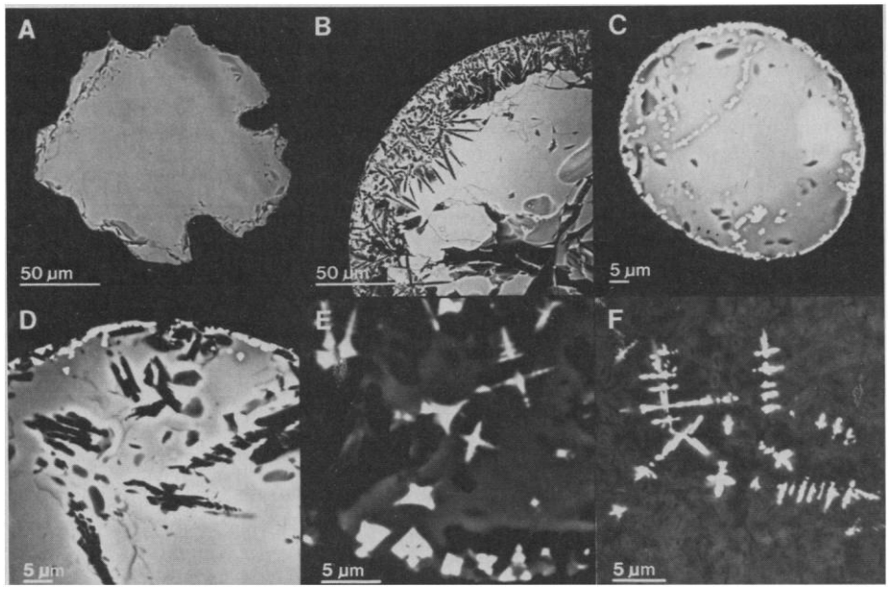

Fig. 2. Scanning electron micrographs in the backscattered mode of polished sections of late Pliocene glassy spherules and a spherule from the K-T boundary of Petruccio, Italy. (**A**) Microtektite-like object shown in Fig. 1E, with deep etching and pure glass composition. (**B**) Spherule with etched holes suggestive of dissolved spinifex olivine crystals and scattered spinel crystals along the outer rim. (**C**) Glassy spherule with spinel mainly on the rim and near the center. (**D**) Glassy spherule with spinel on the rim and olivine dissolution. (**E**) Close-up of a spherule showing the detailed morphology of skeletal spinel crystals; this morphology is indicative of rapid crystallization. (**F**) Section of a spherule from the K-T boundary of Petruccio, Italy, with skeletal spinel crystals similar to those in (E); the original glassy matrix is now altered to glauconite (sample provided by S. Montanari).

boundary spherules (Table 1) cannot be a coincidence. Although these impact events differ greatly in magnitude, both have produced remarkably similar deposits with high concentrations of Ir (*3*) and trace amounts of spherules. As in the late Pliocene deposits, K-T boundary spherules typically constitute <1% of the total sediment (*8*) and not all spherules contain spinels (*14*). The Ni-rich magnesioferrite compositions of these spinels have not been reported in other deposits and imply that they formed under similar conditions. The K-T boundary spinels must be relict mineral grains formed during an impact event (*15*). Furthermore, they probably crystallized from spherules with mafic compositions and thus indicate that either the K-T projectile or the impact target had a mafic component (for example, oceanic lithosphere).

REFERENCES AND NOTES

1. F. T. Kyte, Z. Zhou, J. T. Wasson, *Nature* **292**, 417 (1981).
2. F. T. Kyte and D. E. Brownlee, *Geochim. Cosmochim. Acta* **49**, 1095 (1985).
3. F. T. Kyte, L. Zhou, J. T. Wasson, *Science* **241**, 63 (1988).
4. Spherules were recovered from previously analyzed samples of E13-3 (magnetic separates) and E13-4 (fine fractions). We have not attempted to recover spherules from E10-2, the only other core with known impact debris (*3*). A single bulk sample of ~100 spherules with a mass of 0.6 mg was analyzed by NAA, primarily to determine the Ir content of the spherules. Analytical uncertainties for the NAA data are ±10 to 15%. Another ~100 spherules have been individually examined in a scanning electron microscope to characterize surface textures. Twenty-four spherules representing the spectrum of exterior morphologies were cut into polished sections to characterize interior textures and mineralogy by quantitative major element analyses with an electron microprobe.
5. S. V. Margolis, V. Barnes, P. Cloud, R. V. Fisher, *Proc. Lunar Sci. Conf.* **2** (part 1), 909 (1971); B. P. Glass, *Geol. Soc. Am. Bull.* **85**, 1305 (1974).
6. Because the size of most spinel crystals is below the limit of resolution of the electron microprobe, quantitative analyses were difficult to obtain. We used the abundance of Si as a measure of contamination of the analysis because it was clear that measurable Si indicated excitation of surrounding glass. We report only analyses in which SiO_2 concentrations were <1.5%, but these are representative of all spinels. More than 100 individual spinel crystals were analyzed in 24 separate spherule polished sections. All spinels showed similar enrichment in Ni, Cr, and Mg and low Ti.
7. S. E. Haggerty, *Short Course Notes* (Mineralogical Society of America, Washington, DC, 1976), vol. 3, p. Hg 101.
8. J. Smit and F. T. Kyte, *Nature* **310**, 403 (1984).
9. F. T. Kyte and J. Smit, *Geology* **14**, 485 (1986).
10. B. F. Bohor, E. E. Foord, R. Ganapathy, *Earth Planet. Sci. Lett.* **81**, 51 (1986).
11. E. Doehne and S. V. Margolis, *Geol. Soc. Am. Spec. Pap.*, in press.
12. T. N. Irvine, *Can. J. Earth Sci.* **2**, 648 (1968).
13. B. P. Glass and C. A. Burns, *Proc. Lunar Planet. Sci. Conf.* **18**, 455 (1988).
14. A. Montanari *et al.*, *Geology* **11**, 668 (1983).
15. Spherules are a nearly ubiquitous component in K-T boundary sediments and have a variety of mineral compositions (*13*). Several researchers have argued that they have a nonimpact origin; for example, H. R. Naslund, C. B. Officer, G. D. Johnson, *Geology* **14**, 923 (1986); G. A. Izett, *Geol. Soc. Am. Bull.* **99**, 78 (1987). Our results specifically apply only to spinel-bearing spherules in the K-T boundary, but the impact association is clear.
16. Curation of Eltanin cores is supported by the National Science Foundation (NSF). We are indebted to A. Kaharoeddin and D. S. Cassidy for assistance in obtaining sediment samples. This research was supported by NSF grant EAR-8904833 and a grant from the Institute of Geophysics and Planetary Physics–Lawrence Livermore National Laboratory.

30 October 1990; accepted 31 January 1991

Characterization of a Human TAR RNA–Binding Protein That Activates the HIV-1 LTR

ANNE GATIGNOL, ALICIA BUCKLER-WHITE, BEN BERKHOUT, KUAN-TEH JEANG*

Human immunodeficiency virus type 1 (HIV-1) gene expression is activated by Tat, a virally encoded protein. Tat trans-activation requires viral (trans-activation–responsive; TAR) RNA sequences located in the R region of the long terminal repeat (LTR). Existing evidence suggests that Tat probably cooperates with cellular factors that bind to TAR RNA in the overall trans-activation process. A HeLa complementary DNA was isolated and characterized that encodes a TAR RNA–binding protein (TRBP). TRBP activated the HIV-1 LTR and was synergistic with Tat function.

REGULATORY MECHANISMS INITIALLY described for viral systems often provide the first clue for the existence of counterpart mechanisms in cells (*1*). For example, recent molecular studies on HIV-1 have resulted in the description of novel modes of gene expression. There is compelling evidence that HIV-1 Tat and Rev proteins regulate viral transcriptional and posttranscriptional events through targeted RNA sequences (*2–6*). In particular, the association of Tat with TAR RNA (*7–9*) allows Tat to position itself optimally so as to activate DNA promoter sequences (*10, 11*). This process, which involves a bipartite DNA-RNA target, has yet to be demonstrated for a cellular transcription factor.

The HIV-1 TAR sequence is located between nucleotides +19 and +42 (+1 is defined as the transciptional start point) in the R region of the LTR (*7*). TAR RNA can fold into a stable stem-bulge-loop structure (*4*). Mutations that disrupt the stem, affect the loop or bulge, or destroy the overall secondary structure of the RNA interfere with Tat trans-activation (*5, 6, 12, 13*). Thus, a correct Tat-TAR interaction is essential for optimal expression of the LTR. Cell type–specific experiments, however, suggest that this interplay between Tat and TAR is not sufficient to explain the complete trans-activation process. The observation that Tat activates the HIV-1 LTR poorly in mouse (*14*) and hamster (*15*) cells as compared to human cells has led to the proposal that cellular proteins are important accessories in Tat trans-activation. Several human proteins that bind to TAR RNA have been identified (*16*); however, it is difficult to study the function and similarity of these proteins until the genes encoding them are isolated. We report here the characterization of a human cDNA sequence that encodes for a TAR RNA–binding protein that trans-activates the HIV-1 LTR.

To obtain cDNAs that code for TAR RNA–binding proteins we assayed a HeLa cell library with an RNA recognition site probe. This approach incorporated a modification of the procedure used to identify sequence-specific DNA-binding proteins (*17*). We substituted a uniformly ^{32}P-labeled TAR RNA in place of a DNA probe. This TAR RNA probe was used to screen a λ ZAP cDNA expression library (*18, 19*). In principle, all phage plaques that contain TAR RNA–binding proteins should bind the probe and become radioactively labeled. In the first round of "plaque hybridization" many plaques became radioactively labeled. We purified one plaque to homogeneity through two successive rounds of dilution and rescreening.

We characterized this cDNA clone in two ways. First, the insert, TRBP, was excised from the phage vector and completely sequenced. TRBP contains an open reading-frame, sufficient for 345 amino acids, that is positioned directly in frame to the β-galactosidase gene in λ ZAP (Fig. 1) (*18*). Thus TRBP (with a predicted size of 36,949 daltons) is expressed in this vector as a 44-kD fusion protein consisting of 402 amino acids. We then transferred the TRBP cDNA as a plasmid into *Escherichia coli* XL1 blue (*18*). In this setting, we could induce the fusion protein using isopropyl-1-thio-β-

Laboratory of Molecular Microbiology, National Institute of Allergy and Infectious Diseases, National Institutes of Health, Bethesda, MD 20892.

*To whom correspondence should be addressed.